NASA/TM–20250008157

Acoustic Evaluation of the High Resolution Traversing Microphone Array

Kelly M. Shelts
Matthew B. Galles
Ian A. Clark
Nikolas S. Zawodny
Langley Research Center, Hampton, Virginia

December 2025

NASA STI Program Report Series

Since its founding, NASA has been dedicated to the advancement of aeronautics and space science. The NASA scientific and technical information (STI) program plays a key part in helping NASA maintain this important role.

The NASA STI Program operates under the auspices of the Agency Chief Information Officer. It collects, organizes, provides for archiving, and disseminates NASA's STI. The NASA STI Program provides access to the NTRS Registered and its public interface, the NASA Technical Report Server, thus providing one of the largest collections of aeronautical and space science STI in the world. Results are published in both non-NASA channels and by NASA in the NASA STI Report Series, which includes the following report types:

- TECHNICAL PUBLICATION. Reports of completed research or a major significant phase of research that present the results of NASA programs and include extensive data or theoretical analysis. Includes compilations of significant scientific and technical data and information deemed to be of continuing reference value. NASA counterpart of peer-reviewed formal professional papers, but having less stringent limitations on manuscript length and extent of graphic presentations.
- TECHNICAL MEMORANDUM. Scientific and technical findings that are preliminary or of specialized interest, e.g., quick release reports, working papers, and bibliographies that contain minimal annotation. Does not contain extensive analysis.
- CONTRACTOR REPORT. Scientific and technical findings by NASA-sponsored contractors and grantees.
- CONFERENCE PUBLICATION. Collected papers from scientific and technical conferences, symposia, seminars, or other meetings sponsored or co-sponsored by NASA.
- SPECIAL PUBLICATION. Scientific, technical, or historical information from NASA programs, projects, and missions, often concerned with subjects having substantial public interest.
- TECHNICAL TRANSLATION. English-language translations of foreign scientific and technical material pertinent to NASA's mission.

Specialized services also include organizing and publishing research results, distributing specialized research announcements and feeds, providing information desk and personal search support, and enabling data exchange services.

For more information about the NASA STI Program, see the following:

- Access the NASA STI program home page at `http://www.sti.nasa.gov`
- Help desk contact information: `https://www.sti.nasa.gov/sti-contact-form/` and select the "General" help request type.

NASA/TM–20250008157

Acoustic Evaluation of the High Resolution Traversing Microphone Array

Kelly M. Shelts
Matthew B. Galles
Ian A. Clark
Nikolas S. Zawodny
Langley Research Center, Hampton, Virginia

National Aeronautics and
Space Administration

Langley Research Center
Hampton, Virginia 23681-2199

December 2025

Available from:

NASA STI Program / Mail Stop 150
NASA Langley Research Center
Hampton, VA 23681-2199

Abstract

The High Resolution Traversing Microphone Array (HiRTMA) represents a significant advancement in experimental capabilities for acoustics research at the NASA Langley Research Center. This paper describes the setup of the HiRTMA and acoustic validation experiments performed to verify the HiRTMA's functionality. The array consists of a large structural frame that supports a rotation stage with an attached arc-shaped structure instrumented with 31 microphones. The microphones are spaced at 6° increments along the 12-foot diameter arc, and the entire arc can rotate about the test article to enable hemispherical acoustic measurements. For this validation experiment, the array was assembled in the anechoic chamber of the Structural Acoustics Loads and Transmission (SALT) Facility and tested with multiple well-documented noise sources. The measurements acquired by the HiRTMA showed excellent agreement with published results for a broadband airball source, reference sound source, and a dodecahedron speaker with an equalized pink noise signal, demonstrating the HiRTMA's suitability for characterizing various acoustic sources. Results illustrating the effects of geometric recentering algorithms are also presented. The results presented here validate the HiRTMA Array at the NASA Langley Research Center as a suitable measurement apparatus for hemispherical acoustic measurements.

1 Introduction

Aircraft noise continues to be a problem for communities near airports. The National Aeronautics and Space Administration (NASA) has been studying aircraft acoustics and noise reduction methods for decades [1–3]. Many of these studies involve experiments to test acoustic theories and increase understanding of noise-generating mechanisms. To ensure that the acoustic measurements are free from reflections and external noise sources, many studies are performed in anechoic chambers that simulate acoustic free-field conditions. One such facility is the anechoic chamber at the Structural Acoustics Loads and Transmission (SALT) Facility at the NASA Langley Research Center.

While facilities like SALT are highly effective, they are not without limitations. Acoustic measurement areas are often constrained by hardware and available space, restricting the number and placement of microphones. Many studies utilize stationary microphones on stands, which allows customized setups, but limited coverage. In addition, microphone phased arrays and beamforming techniques are often used to identify noise sources. However, these techniques often lack the geometric resolution needed to measure complex source directivity. To address these challenges, many research organizations have developed custom experimental setups to enable high-resolution directivity measurements for specific applications [4–6]. These often consist of microphones arranged spherically around a stationary source, or along an arc centered on the source, with a complete directivity sweep obtained by rotating either the source or the arc.

Inspired by these approaches, an effort was launched at NASA Langley to develop an acoustic-directivity-measurement system designed for studies of aircraft acoustics. The High Resolution Traversing Microphone Array (HiRTMA) was created to address some of these limitations. The HiRTMA provides the capability to acquire acoustic measurements for an entire hemisphere with 6-foot radius at 3° polar angle resolution, using 31 microphones positioned on an arc that rotates around the test article, as shown in Figure 1.

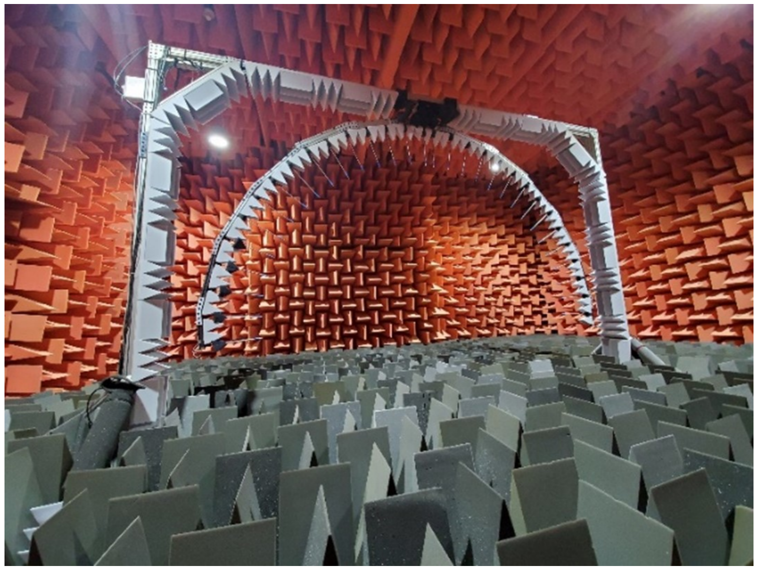

Figure 1. High Resolution Traversing Microphone Array in the Structural Acoustics Loads and Transmission (SALT) Facility.

NASA acoustics researchers advised an undergraduate student design team from Virginia Polytechnic Institute and State University that was tasked with the initial design and fabrication of the HiRTMA [7]. After delivery to NASA, the HiRTMA's behavior was assessed using well-documented noise sources. This assessment also provided an opportunity to define operating procedures and determine applicability for future experiments.

The purpose of this document is to provide a record of the steps that were taken to make the HiRTMA functional and demonstrate its basic capabilities for consideration in future tests. The rest of this paper is organized as follows: Section 2, HiRTMA, describes the array design, installation procedures, microphone positioning, and reflection mitigation. Section 3, Experimental Methods, describes the test facility, coordinate system, control system, data processing, sound sources, and test procedures used in this work. Section 4 presents the measured results and comparisons to manufacturer specifications and results obtained with other measurement systems.

2 HiRTMA

Developing the HiRTMA to an operational state required extensive effort and troubleshooting due to its innovative design and complexity. As a new piece of hardware with a unique control system and a significantly larger array of microphones than previously utilized in the SALT Facility, the HiRTMA presented numerous technical challenges. This section details the setup and refinement of the HiRTMA, including its design, installation, microphone placement, and reflection control measures.

2.1 Array Design

The primary structure of the HiRTMA array is made of T-slot aluminum extrusion, as shown in Figure 2. The vertical supports are 14 feet tall and consist of 3-inch × 6-inch sections connected with structural brackets and mounting fasteners. The top beam consists of parallel 1.5-inch × 3-inch sections oriented vertically, with 3-inch-long, 1.5-inch × 3-inch sections installed between them to provide additional support. Lengthwise, the top beam is split into three sections—two 46.5-inch-long sections and a 10-foot-long section in the center, from which the rotation stage is suspended. Two 32-inch-long angled sections are mounted to the vertical supports and the top beam to add rigidity to the structure.

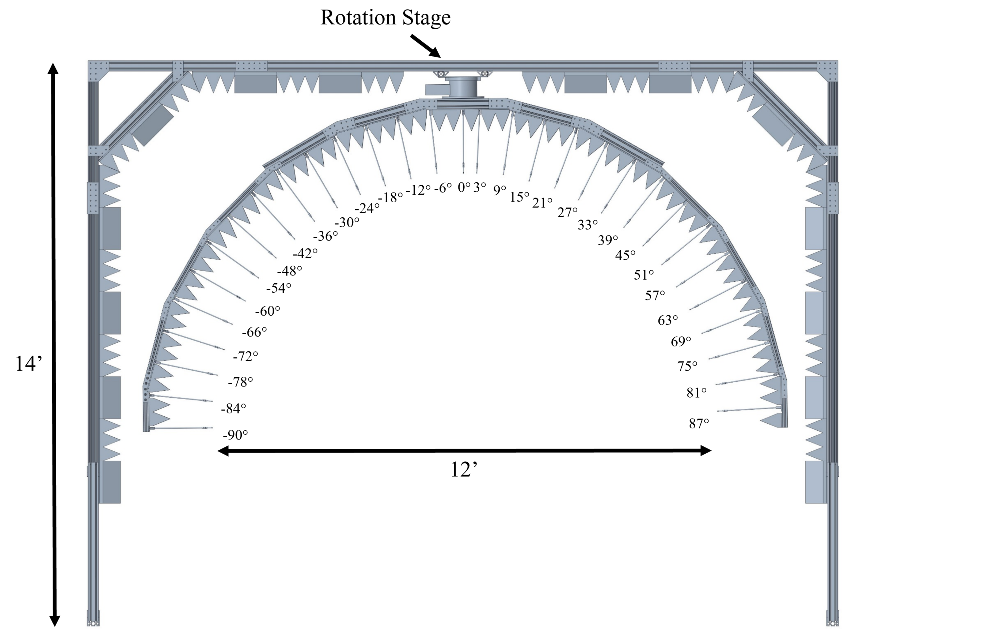

Figure 2. HiRTMA geometry, with polar angles of microphones illustrating the microphone offset enabling a 3-degree polar angle resolution with full rotation of the array.

The arc is made of 1.5-inch by 1.5-inch aluminum T-slot beams cut at angles and connected with brackets to form a 14-foot, 4-inch diameter semicircle. The lowest three sections on each side of the arc are made of plastic extrusion with equivalent dimensions to reduce weight and minimize drooping. Thirty-one microphone holders are installed along the arc, each comprised of three components: a 3D-printed microphone holder with a nylon-tipped set screw, a 14-inch aluminum tube, and a 3D-printed base that holds the tube at an angle so the microphone points toward the center of the arc. This offset angle is necessary because the arc is formed from straight segments. When installed, the microphone tips form a 6-foot radius semicircle. The microphones are placed every 6° along the arc, with a 3° asymmetric offset on one side, so that a complete ±180° rotation yields 3° polar resolution. Melamine foam wedges were installed on all internal surfaces of the HiRTMA frame and arc to reduce reflections. Additional detail about acoustic treatment is presented in Section 2.4.

2.2 Assembly

The HiRTMA structure was assembled in three main components—the two vertical supports and the top beam. During setup, temporary angled supports were installed to brace the vertical supports for additional stability, as illustrated in red in Figure 3. Then, the top beam with the rotation stage installed was lifted into position by two manual lifts. After which, the vertical supports were brought in and then attached to the top beam before the manual lifts were removed. After discussions with NASA safety personnel, this procedure was determined to be the safest process to assemble the array. After the vertical supports were installed, the arc was installed section by section, to reduce the amount of weight the operator would need to support and to avoid an uneven load on the rotation stage. After the assembly of the HiRTMA, the temporary braces on the inside of the structure were removed while the temporary braces on the outside of the structure were left in place.

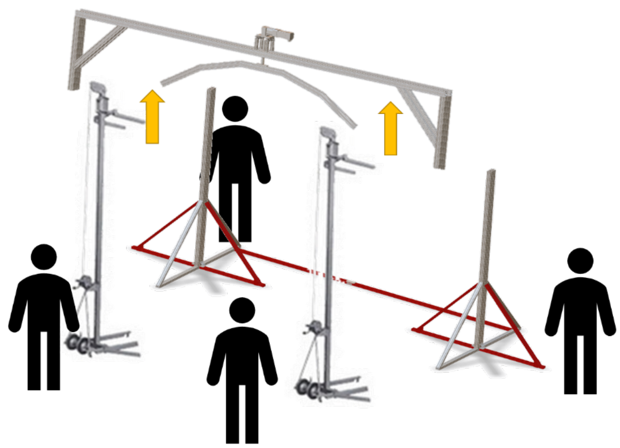

Figure 3. Assembly of the HiRTMA, with two team members using lifts to position the center section while two others align the support legs for attachment.

The microphone cables were installed after the arc was assembled, with the cables running from their location on the arc, then bundled near the 0° mic and routed on top of the top beam and around the vertical support nearest the chamber door. The cables were bundled with sufficient slack to allow the array to rotate ±180°, and wrapped with protective plastic casing to prevent wear on the cables. The acoustic foam wedges were glued to balsa wood panels with hook-and-loop fasteners on the structure-facing side so they could be affixed after the structure was assembled.

2.3 Microphone Positioning

A laser scanner was used to accurately measure the geometry of the array hardware. The laser scanner was placed at multiple positions around the array and the measured point clouds were combined within the scanner software to increase the fidelity of the final result, as shown in Figure 4.

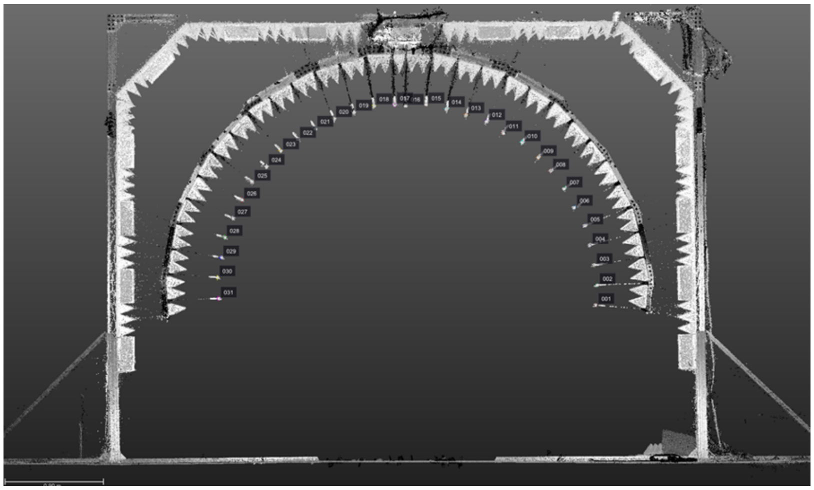

Figure 4. Compiled point cloud from laser scans of the HiRTMA with microphone tip locations identified.

The scanning system included sphere detection capability, so spherical microphone caps were designed and 3D printed, where the microphone tip was located at the center of the sphere, as shown in Figure 5a. These spherical caps had an outer diameter of 1-inch, and fit over the microphone grid caps. Vent ports were included on the spherical caps to prevent excessive air pressure changes on the microphone diaphragm upon installation and removal.

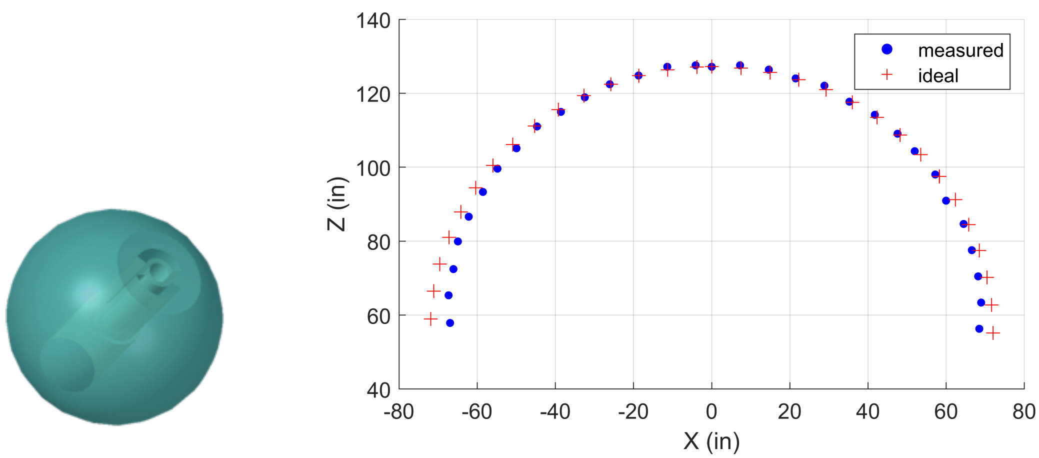

(a) (b)

Figure 5. (a) Spherical microphone covers used to measure microphone position and (b) comparison between measured and design-specified microphone positions, illustrating arc deviation of up to five inches.

The microphone positions from the laser scan were compared with the designed positions, as shown in Figure 5. The 0° microphone was used as a reference point for the other positions. Microphone positions deviated from the design due to a combination of structural sag and connection variability in the bracket assemblies. The lowest arc positions deviated up to 5 inches from their nominal positions. This deviation was accounted for in post-processing by applying an inverse-square-law amplitude correction using the actual microphone to source distances, assuming that variations in microphone sensitivity due to off-axis incidence were negligible. The maximum amplitude correction due to the droop was 0.6 dB.

2.4 Reflection Mitigation

Acoustic reflections were anticipated when designing the HiRTMA array. Preliminary mitigations included installing melamine foam acoustic wedge treatment on the internal surfaces of the array structure, as shown in Figure 1. To assess the effectiveness of this treatment, sound was generated using the broadband pressurized air source, the airball (more detail in 3.5). The source was mounted in upward and sideways orientations, and pointing toward the frame structure and pointing toward the arc. Reflections were identified using the normalized autocorrelation, R_{xx}, of each microphone signal, as described in Equation 1. [8,9]

$$R_{xx}[k] = \frac{\sum_n x[n] \cdot x[n+k]}{\sum_n x[n]^2} \tag{1}$$

Here, $x[n]$ is the zero-mean, bandpass-filtered pressure signal from a given microphone, n is the sample index, and k is the lag index, representing the number of samples by which the signal is shifted. The autocorrelation is normalized such that $R_{xx}[0] = 1$, and all other values satisfy $|R_{xx}[k]| \leq 1$. Reflections appear as secondary peaks in $R_{xx}[k]$ at nonzero time lags, indicating delays in the arrival of reflected sound waves. The location of the reflecting surface is determined by multiplying the delay time by the local speed of sound to calculate the propagation distance of the reflected acoustic waves.

A reflection was identified originating from the base of the microphone holder, where it was attached to the arc. To address the gap in acoustic treatment at this location, dark gray pyramidal acoustic foam was added around the microphone extension tube, as illustrated in Figure 6. Figure 7a shows the time-domain autocorrelation for a single microphone on the original arc configuration without additional foam at the base of the microphone holder (red) and the same microphone with added acoustic foam treatment (black). In the untreated case, secondary peaks between 2 and 3 milliseconds indicate reflections from the base of the microphone holder where it connects to the arc structure, as shown in Figure 6. The time delay of these peaks corresponds to the additional distance the reflected wave travels, based on the speed of sound. Adding acoustic foam at this location significantly reduced the amplitude of these reflections, as shown by the diminished peaks in the black curve.

Figure 7b shows the narrowband SPL values in the frequency domain before and after additional acoustic treatment was added. The reflection caused spectral ripple in the frequency domain acoustic measurements, and the resulting spectrum exhibits more amplitude variation with frequency. With additional acoustic treatment, the spectrum is smoother, with less amplitude variation. No other repeatable reflections were identified.

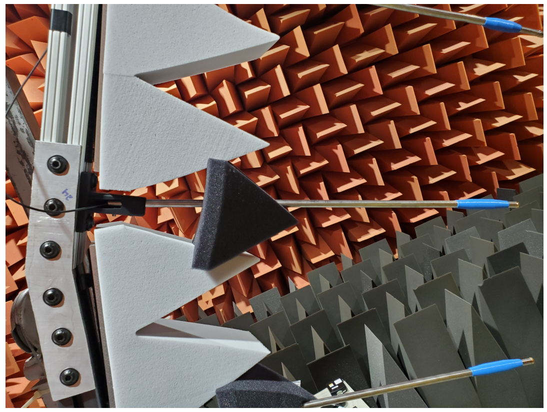

Figure 6. Dark gray acoustic foam added to the microphone array mitigates reflections from the microphone holder mount.

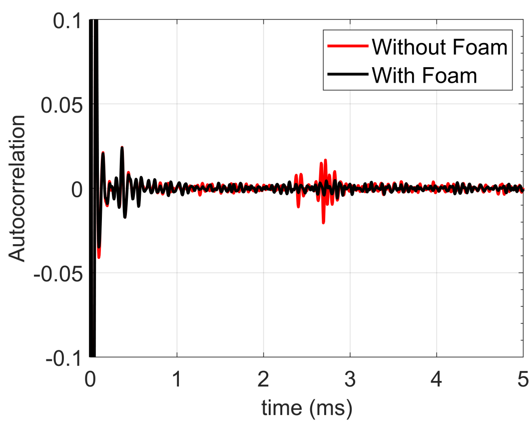

(a)

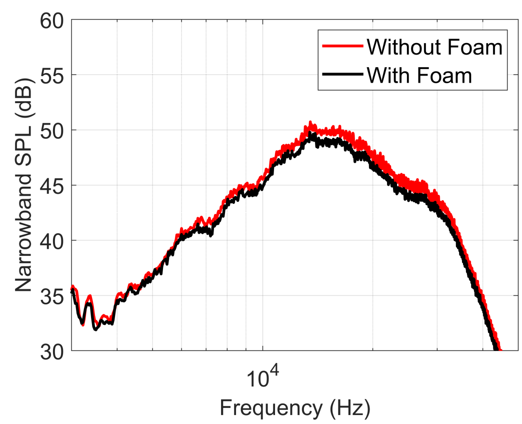

(b)

Figure 7. Reflection mitigation effects of additional foam on microphone holder base in the (a) time domain and (b) frequency domain.

3 Experimental Methods

The following section outlines the experimental methods employed in this study. It includes detailed descriptions of the test hardware, measurement system, facility setup, and procedures used to acquire and process the acoustic data.

3.1 The SALT Facility

The SALT facility at NASA Langley Research Center is a state-of-the-art reverberant-anechoic test suite designed for a wide range of acoustic experiments. For this study, the experiment was conducted in the anechoic chamber, which has dimensions of 30 feet long, 25 feet wide, and 17 feet high. The chamber is specifically designed to minimize reflections, with the floor, ceiling, and walls treated with 3-foot-tall open-cell polyurethane foam wedges, ensuring an environment that simulates free-field radiation conditions for frequencies above 80 Hz [10, 11]. This setup provides an ideal testing environment to accurately measure acoustic phenomena without interference from unwanted reflections, allowing for precise analysis of noise sources and directivity patterns.

3.2 Coordinate System

Measurement locations are defined in terms of microphone angle along the HiRTMA arc and the rotation angle of the arc (azimuthal angle), set by the motor controller. These correspond to polar and azimuthal angles in a spherical coordinate system centered at the test article. Microphone angles vary from -90° to 87°, as shown in Figure 2. Because the microphone angles are interspaced to provide 3° of resolution, measurements are combined and labeled with polar angles from 0° to 90° for contour plots, as shown in Figure 8, where 0° corresponds to the microphone in the center of the arc, and 90° corresponds to the lowest microphone position. Azimuthal angle varies from 0° to 360° circumferentially, corresponding to rotation of the arc around its center. For each source, the microphone arc was rotated about its azimuth at 10° increments, then the motor was disabled before data acquisition.

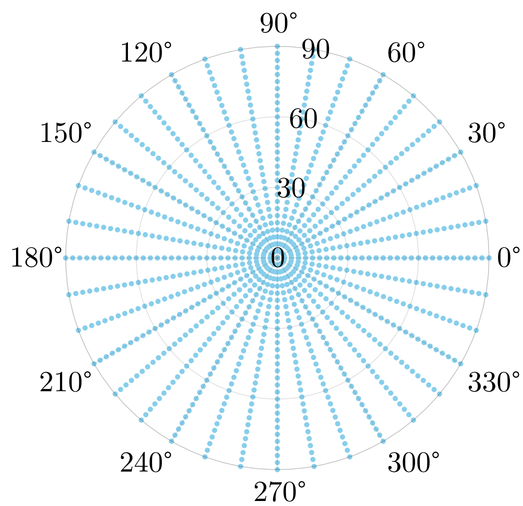

Figure 8. HiRTMA measurement locations projected onto a flat plane.

3.3 Control System

A motor controller and motorized rotation stage are used to rotate the array about its azimuth. Motion routines and motor feedback settings are defined within the controller's software. Because of the large inertia of the arc, the motor was tuned manually, rather than relying on the in-built tuning schemes that are inappropriate for such a large structure. Although a direct-drive system would be preferred for the large inertia loads of the HiRTMA arc, the geared rotation stage was used because it was available in lab inventory and met the necessary performance criteria. If future upgrades were considered, a direct-drive option would be recommended. Vibration effects and settling time were determined using accelerometers attached with mounting wax to the lowest point of the arc structure.

To minimize arc vibration, the motion routines were adjusted to move the array slowly (1°/sec), with 50% s-curve ramp-up and ramp-down profiles to reduce settling time.

The motor controller uses a 20 kHz signal to communicate with the motor, which was found to cause electromagnetic interference and contaminate the microphone measurements when enabled. To mitigate this, the motor was disabled before data acquisition.

3.4 Acoustic Data Processing

For the plots shown in this report, the array was instrumented with Brüel & Kjær 4954B microphones—1/4-inch free-field, prepolarized microphones designed for high-level and high-frequency measurements, with a dynamic range of 40-159 dB and frequency response from 16 Hz to 80 kHz. An additional microphone used for diagnostic purposes was mounted on a stand that was 12 feet from the center of the arc, at a rotation angle of 45 degrees. Its measurements are not shown in this paper.

The microphones were connected to a data acquisition system and acquired data at a rate of 204,800 samples per second for 10 seconds for all data shown in this paper. The frequency spectrum was calculated using Welch's method with a spectral bin width of 32 Hz and a Hanning window with a 50% overlap between time-history segments. Pistonphone calibrations at 251.2 Hz were used to determine the individual microphone sensitivities for converting the output from volts to pascals. Measured sound pressure levels in dB (SPL_m) were calculated from the pressure readings with a reference pressure of 20 μPa.

Adjustments were applied to the SPL data to account for atmospheric absorption, individual microphone frequency response, and slightly varying distances from the microphone to the source. Atmospheric corrections, (C_{atm}), were calculated using ANSI S1.26-1995 with in-chamber temperature, pressure, and humidity readings to correct microphone measurements to standard atmospheric conditions. [12]. For all microphones, the reference sensitivity at 251.2 Hz was established using a pistonphone calibrator. To determine the frequency-dependent sensitivity variations, each microphone was characterized with an electrostatic actuator, which applies a calibrated excitation across a wide frequency range. This process generated a frequency response curve relative to the 250 Hz reference sensitivity (C_{el}). To account for varying microphone distances caused by drooping in the arc structure, an inverse square law correction was applied, (C_d). The final microphone response, (SPL_f), is calculated by adding these corrections to the as-measured frequency response, (SPL_m). The complete correction chain can be expressed as:

$$SPL_f(f) = SPL_m(f) + C_{\text{atm}}(f) + C_{\text{el}}(f) + C_{\text{d}}(\Phi, \theta). \tag{2}$$

The free-field responses for each microphone when actuated by the electrostatic actuator, relative to the response at 251.2 Hz, are shown in Figure 9. At frequencies between 100 and 1000 Hz, the free-field responses across the 31 microphones installed on the HiRTMA were largely consistent. At higher frequencies, significantly different trends in frequency response were observed, which were attributed to different manufacturing batches produced years apart. It was observed that microphones with sequential serial numbers had similar frequency response trends, but these trends differed between manufacturing batches produced years apart. This variation in frequency response was up to ±2 dB at frequencies between 4 kHz and 80 kHz, which is within the expected variation specified by the manufacturer.

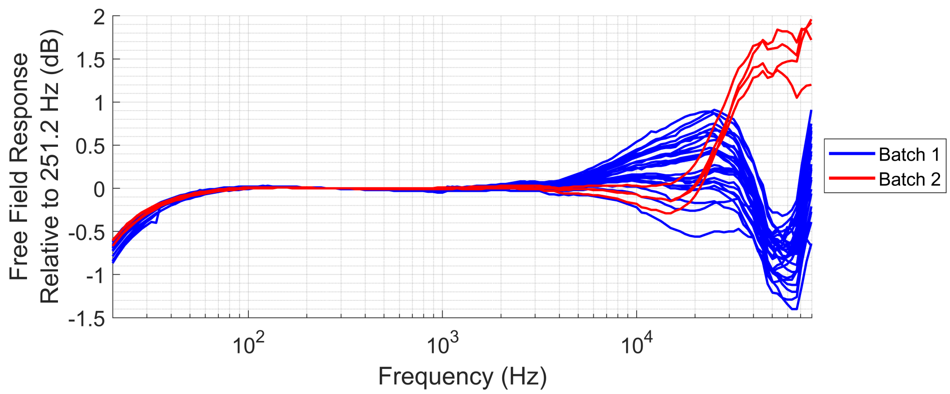

Figure 9. Electrostatic actuator response for 31 microphones on the HiRTMA.

Applying the free-field response corrections to the measured data accounted for these individual microphone characteristics and smoothed the irregularities caused by microphone-to-microphone variations. Figure 10 shows one-twelfth-octave band SPL contours centered around 60 kHz for a broadband sound source before and after the electrostatic frequency response corrections are applied. In this paper, 12th octave SPL is used as a shorthand for sound pressure levels generated in one-twelfth-octave bands. Adjusting for the individual microphone response removes data features due to these variations, such as the higher sound level shown at 30° polar angle and oscillatory amplitudes between the 50° and 70° polar angles. Figure 10b shows continuous decreases in SPL beyond 30° polar angle.

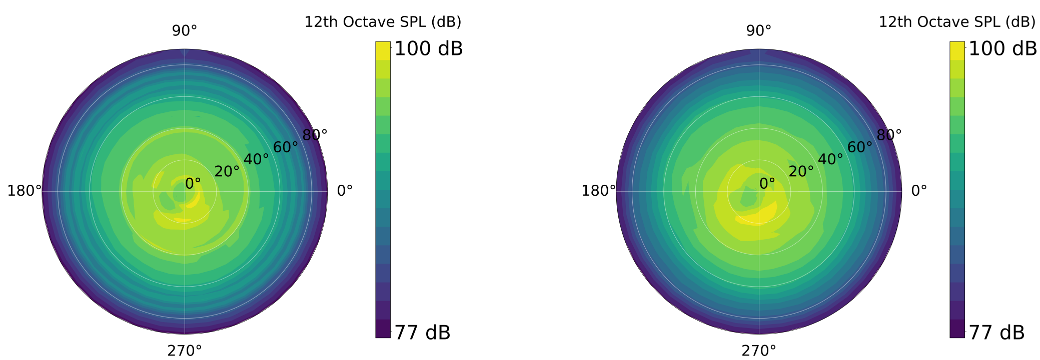

(a) Before electrostatic frequency response correction is applied.

(b) After electrostatic frequency response correction is applied.

Figure 10. 60 kHz one-twelfth-octave band SPL contours for a broadband noise source.

3.5 Noise Sources

The HiRTMA array is designed for use with noise sources of varying size, sound amplitude, and frequency range. To assess its suitability for future tests, three sources were used in the characterization: an airball with pressurized air, an Hottinger Brüel & Kjær Reference Sound Source (Type 4204), and a dodecahedron speaker. The airball source was tested in multiple orientations to identify possible reflection sources in the experimental setup—pointing upwards, perpendicular to the frame structure, and toward the array structure. The other sources were tested in a single configuration as shown in Figure 11.

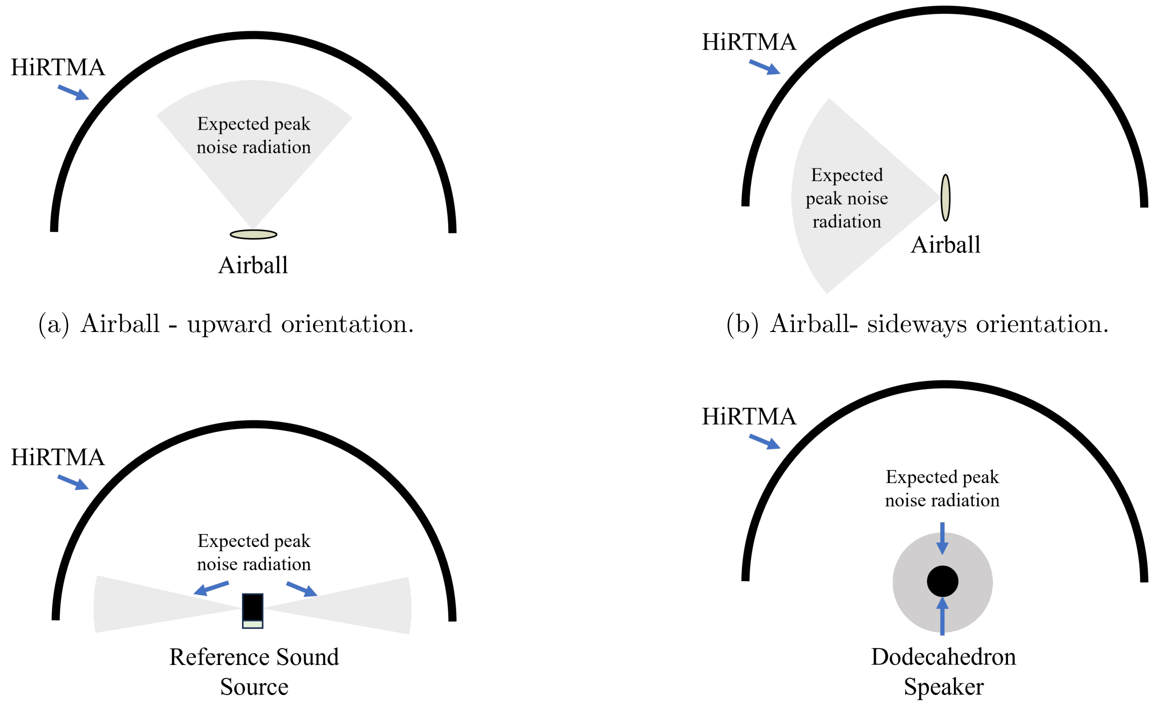

(a) Airball - upward orientation.

(b) Airball- sideways orientation.

(c) Reference Sound Source.

(d) Dodecahedron speaker system.

Figure 11. Acoustic source configurations and expected peak noise radiation zones relative to the HiRTMA arc.

The airball noise source is housed inside a fairing used for in-flow measurements, originally created for a microphone array development study at the NASA Ames Research Center [13]. The fairing is made from selective laser sintering (SLS) using glass-filled nylon and measures 21-inch $\times$ 14-inch and 2 to 3 inches thick (Figure 12). It houses two interchangeable source modules, either tweeter speakers or a 2-inch diameter hemispheric-multi-jet source (airball) operated with pressurized air. The airball has 44 holes, each with a diameter of 0.035 inches in the hemisphere facing the fairing opening, meant to provide an omnidirectional acoustic signature for the hemisphere above the fairing opening. For all cases shown in this document, 16.5 psia of air pressure was used to supply the airball noise source. A porous facesheet was installed to cover the source opening.

The second source, an Hottinger Brüel & Kjær Reference Sound Source (Type 4204), utilizes a centrifugal fan driven by an asynchronous motor to create an axisymmetrically level noise source [14]. The motor uses an external rotor with a high moment of inertia to ensure a constant rotation speed. It is designed to be a repeatable noise source with levels above 70 dB (one-third-octave level) for frequencies between 100 Hz and 20 kHz.

A third source, a dodecahedron speaker set, was used to assess the HiRTMA's ability to measure a low-frequency, omnidirectional source with known directivity. The dodecahedron loudspeaker uses 12 dynamic drivers to create an even sound distribution. Manufacturer

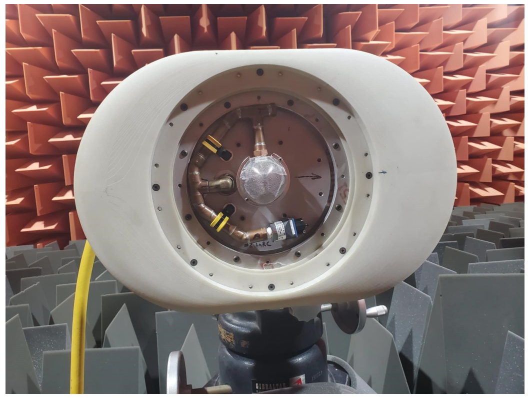

Figure 12. Airball installed in an aerodynamic fairing without the facesheet.

specifications indicate that the directivity is uniform below 1 kHz and a lobing behavior dependent on the individual speaker locations starts at 2 kHz [15]. For the plots presented in this paper, an equalized pink noise signal was used.

3.6 Data Recentering Algorithms

The HiRTMA acquires data over a hemispherical surface centered around a defined point. If the noise source is located at this center (x_i, y_i, z_i), data are acquired at a constant distance and fixed θ and Φ angles (i.e., spherical coordinates) relative to the source, as shown by θ_i and Φ_i in Figure 13. This makes directivity patterns and acoustic behaviors more apparent. If the source of interest is not located at this geometric center, post-processing can be used to reconstruct the data as if it were positioned at the center using coordinate transforms, interpolation, and amplitude corrections. For an offset case, the measured θ_m and Φ_m angles can be calculated knowing the source's actual x_r, y_r, z_r location, as illustrated in Figure 14. Assuming there is sufficient geometric coverage, interpolation between actual and desired θ and Φ can be used to adjust the measured SPL values as though they were acquired with the source in the center. An inverse-square-law distance correction is used to account for the differing distances between source and microphone, making them all as if they were acquired with a 72-inch radius. This correction assumes that the microphones are in the acoustic far field and that variations in microphone sensitivity due to off-axis incidence are negligible.

The trigonometric identity, shown in Equation 3 can be used to determine the measured θ_m and Φ_m angles, as illustrated in Figures 13 and 14. For simplicity, only half of the microphone arc is shown, and the center of the HiRTMA Arc (the ideal source location) is in the center of the coordinate plane. The actual source location is shown in red at x_r, y_r, z_r in Figure 13. The rotation angle of the microphone arc is Φ_i, shown in blue, and the position of the individual microphone along the arc is θ_i, shown in green.

$$\cos\theta = \frac{\mathbf{A} \cdot \mathbf{B}}{|\mathbf{A}|\,|\mathbf{B}|} \tag{3}$$

The vectors required to define measured θ can be defined as $\mathbf{A}$ from (x_r, y_r, z_r) to (x_m, y_m, z_m), shown in purple on Figure 14, and $\mathbf{B}$ from (x_r, y_r, z_r) to (x_m, y_m, z_r), shown in yellow. The vector definitions are shown in Equation 4.

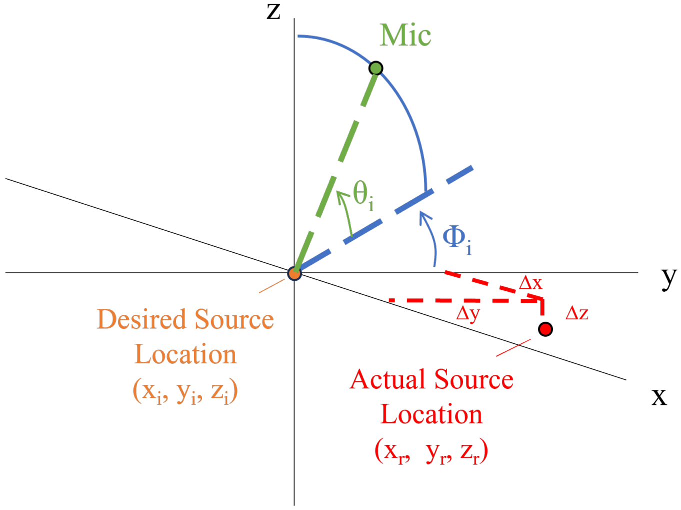

Figure 13. Illustration of geometrical transform to shift measured hemisphere around actual source location.

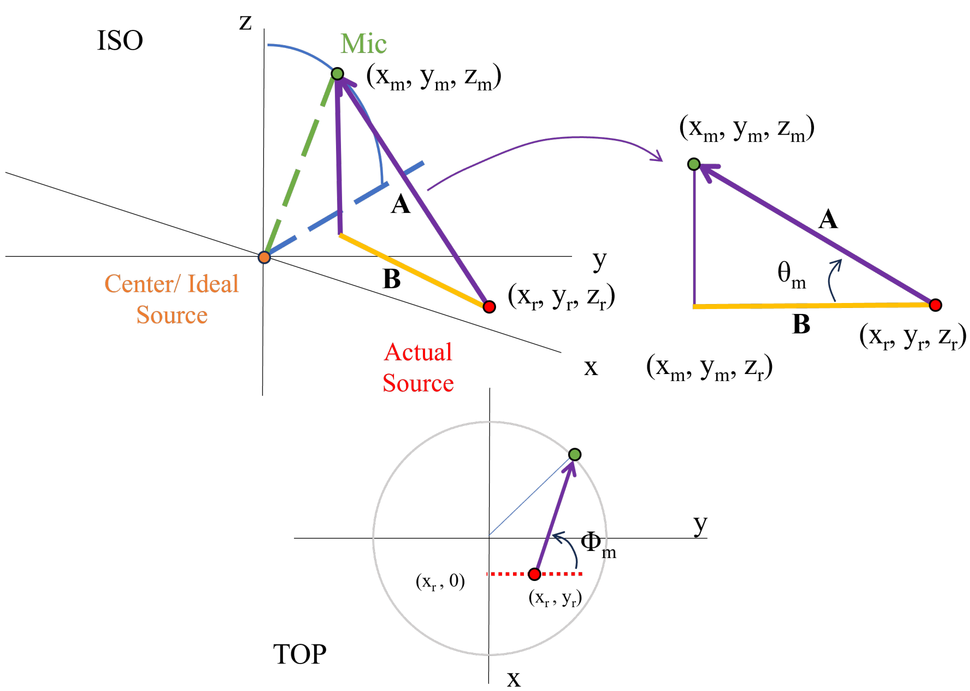

Figure 14. Illustration of vectors to be compared to find θ and Φ.

$$\mathbf{A} = (x_m - x_r,\ y_m - y_r,\ z_m - z_r), \quad \mathbf{B} = (x_m - x_r,\ y_m - y_r,\ 0) \tag{4}$$

The dot product of the vectors and the product of their magnitudes are described in Equations 5 and 6.

$$\mathbf{A} \cdot \mathbf{B} = (x_m - x_r)^2 + (y_m - y_r)^2 + (z_m - z_r) \cdot 0 = (x_m - x_r)^2 + (y_m - y_r)^2 \tag{5}$$

$$|\mathbf{A}| \cdot |\mathbf{B}| = \sqrt{(x_m - x_r)^2 + (y_m - y_r)^2 + (z_m - z_r)^2} \cdot \sqrt{(x_m - x_r)^2 + (y_m - y_r)^2} \tag{6}$$

The final calculation for the angle Θ_m is given by Equation 7. Additional logic is applied afterward to ensure the sign of the angles agree with the HiRTMA's reference system.

$$\Theta_m = \cos^{-1}\left(\frac{(x_m - x_r)^2 + (y_m - y_r)^2}{\sqrt{(x_m - x_r)^2 + (y_m - y_r)^2 + (z_m - z_r)^2} \cdot \sqrt{(x_m - x_r)^2 + (y_m - y_r)^2}}\right) \tag{7}$$

Using the same process, the angle Φ_m can be calculated as the angle between the vectors from (x_r,y_r) to (x_m, y_m), shown in purple in Figure 14, and from (x_r, 0) to (x_r,y_r), shown in red, using the expression shown in Equation 8.

$$\Phi_m = \cos^{-1}\left(\frac{y_m - y_r}{\sqrt{(x_m - x_r)^2 + (y_m - y_r)^2}}\right) \tag{8}$$

The SPL values for the ideal location (θ_i and Φ_i) can be interpolated from (θ_m and Φ_m). Additionally, an inverse-square-law distance correction is applied to account for the change in distance between source and microphone. An example is presented in Section 4.4, where these methods are applied to data measured from an off-center sound source and compared to measured results from a centered sound source.

4 Results

This section presents the acoustic measurements obtained for three sources: the airball, the reference sound source, and the dodecahedron speaker. Data were acquired at 10° resolution azimuthal angles for all cases. The measurements were acquired using the HiRTMA and are compared against previously measured data from other NASA experiments and manufacturer specifications. The comparisons serve to validate the accuracy and reliability of the HiRTMA system while highlighting its performance across different types of sound sources.

4.1 Airball

The airball produces sound levels that increase with frequency, and the airball produces peak SPL near a polar angle of 0° and levels decrease as the polar angle increases. Figure 15 shows one-twelfth-octave band SPL contours at 5, 10, 20, and 60 kHz for the upward orientation. SPL variation on the hemisphere is shown to increase as a function of frequency. At 5 kHz, the area of peak SPL is confined to polar angles below 20 degrees, and increases to 50 degrees for 60 kHz.

The airball's directivity was previously studied at the NASA Ames Research Center. The microphones used in that study were located at a different distance from the source, so an inverse-square-law amplitude correction was applied to account for the difference. One-twelfth-octave band results at 8 kHz are shown in Figure 16. The two experimental setups show good agreement in overall directivity trends—within ±1 dB after distance correction.

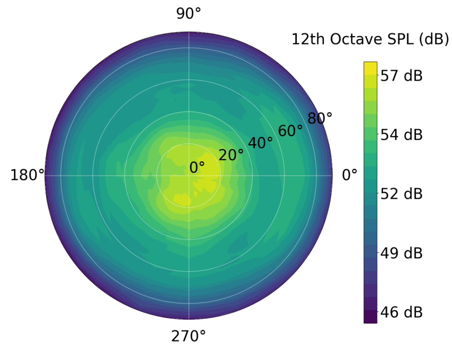

(a) 5 kHz.

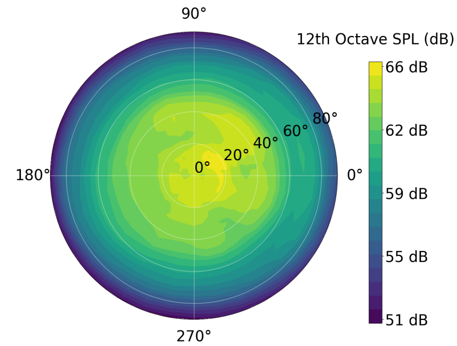

(b) 10 kHz.

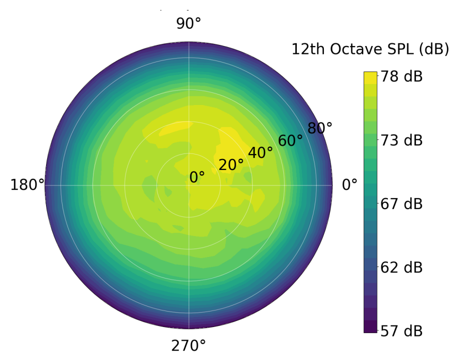

(c) 20 kHz.

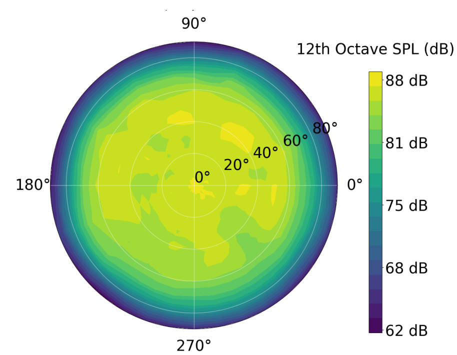

(d) 60 kHz.

Figure 15. One-twelfth-octave band SPL contour plots of airball with 16.5 psi supply air pressure (upward orientation).

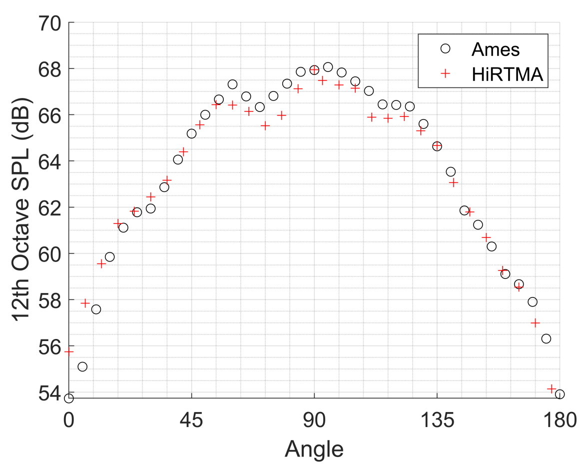

Figure 16. Comparison of one-twelfth-octave band SPL directivity (centered around 8 kHz) to NASA Ames measurements (-90° to 90° arc).

4.2 Reference Sound Source

The reference sound source is a Hottinger Brüel & Kjær Model 4204, which uses a fan to create uniform sound levels circumferentially around the device [14]. For this study, the fan was positioned in the center of the microphone array, directly below the 0° microphone and its height was set so the center of the fan was aligned with the 90° microphone. Figure 17a shows one-twelfth-octave band SPL contours, centered at 8 kHz. The contour plot shows peak noise levels at the 90° microphone, in line with the fan of the Reference Sound Source, with decreasing levels toward the 0° microphone. Figure 17b shows the one-twelfth-octave band SPL values for the 90° microphone at all azimuthal locations (every 10° from 0° to 360°). The levels vary by less than ± 1 dB, verifying the source's circumferential uniformity. These results also verify source stability with time, as measurements were acquired over a 2-hour period with minimal variation.

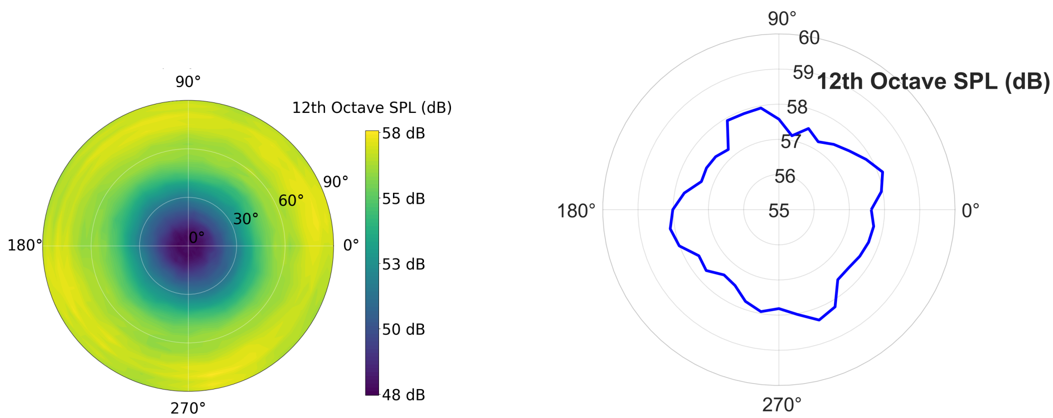

(a) Contour Plot

(b) Polar view of 90° mic SPL

Figure 17. One-twelfth-octave band SPL contour plots centered around 8 kHz for the Reference Sound Source.

4.3 Dodecahedron

For this test, the dodecahedron speaker set played an equalized pink noise signal, and its directivity patterns were clearly visible in the data acquired with the HiRTMA. Figure 18 shows one-twelfth-octave band SPL contours at 500 Hz, 1 kHz, 2 kHz, and 3 kHz for the dodecahedron speaker located in the center of the HiRTMA. At 500 Hz and 1 kHz (Figures 18a and 18b), the sound levels are fairly constant, with ± 1 and ± 2 dB variation, respectively. At 2 and 3 kHz (Figures 18c and 18d), the dodecahedron speaker locations are easily identifiable in the contour plots. Specifically in Figure 18c, the top three speakers show clear increases in sound level at 2 kHz at a polar angle of 30° and azimuthal angles of 0°, 120°, and 240°. This is also apparent for the speakers in line with the 90° polar angle at 60°, 180°, and 300° azimuthal angles. At 3 kHz, as shown in Figure 18d, the interference pattern becomes more complex, and maximum SPLs occur between the speaker locations. The emergence of distinct lobes above 2 kHz demonstrates the value of dense angular sampling (e.g., 3° steps) to avoid spatial aliasing. With a sparser measurement grid, these features would be smeared or entirely missed.

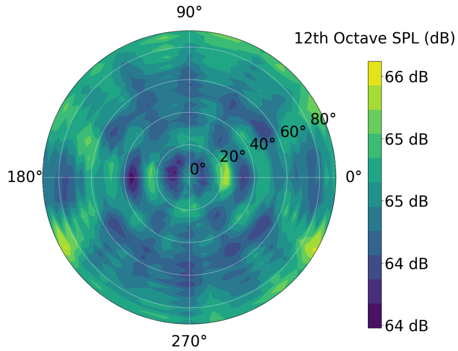

(a) 500 Hz.

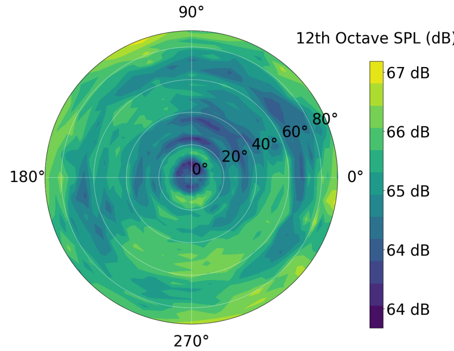

(b) 1 kHz.

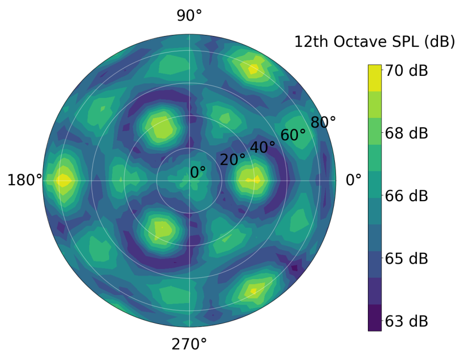

(c) 2 kHz.

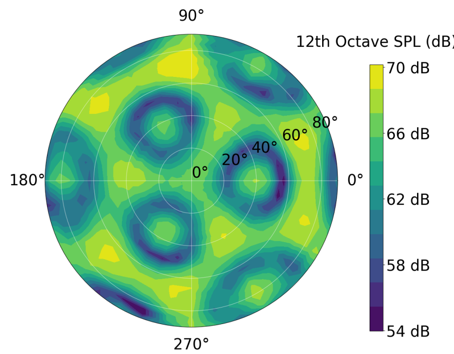

(d) 3 kHz.

Figure 18. One-twelfth-octave SPL contours of the dodecahedron speaker with an equalized pink noise signal between 500 Hz and 3 kHz.

4.4 Data Recentering Algorithms

To demonstrate the effects of the recentering algorithms described in Section 3.6, measurements were acquired for an off-center speaker playing an equalized pink noise signal. The speaker source was oriented upwards and was positioned 18 inches toward the 180° azimuthal angle and 18 inches toward the 90° azimuthal angle, as shown in Figure 19. For this case, the ideal and measured Φ and θ are presented in Figure 20. The measured and desired Φ and θ differ, and there is varying coverage across the desired Φ and θ positions, as shown in Figure 20. However, for many cases, the available geometric distribution is sufficient to interpolate or extrapolate to visualize trends in the data.

The effects of this process are shown in the contour plots in Figure 21. The plots display one-twelfth-octave band SPL values with a center frequency of 4 kHz, normalized to the local maximum. The colorbar axis maximum is 0, and the minimum is the delta from the maximum sound pressure level observed in that dataset. Figure 21a shows the original measurements for the offset speaker case. The peak noise is located around 30° polar angle and 135° azimuthal angle. Because the source is located closer to some microphones, the peak sound levels were higher than for the baseline centered speaker case, shown in Figure 21d. Figure 21b shows the data after the angle interpolation step is performed. The peak SPL is now closer to 0° polar angle, but the levels between azimuthal angles 90° and 180° are

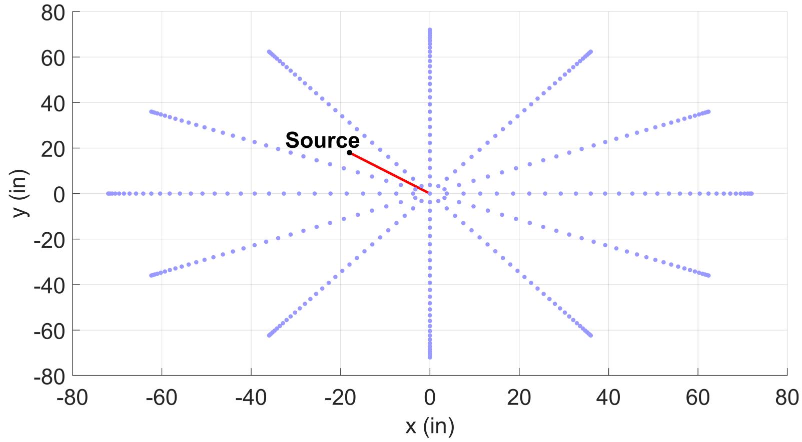

Figure 19. HiRTMA measurement locations relative to actual source location.

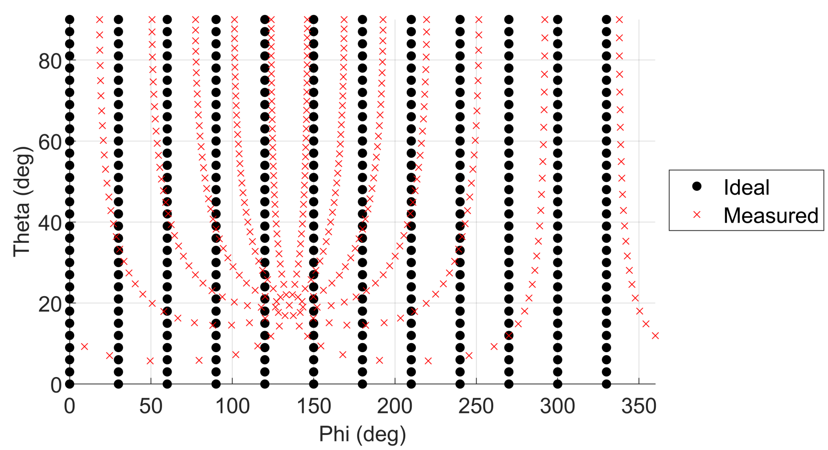

Figure 20. Ideal and measured Φ and θ for interpolation.

higher than the measured case. To resolve this, an inverse-square-law distance correction was applied, using the actual distance between the source and the microphone and the desired distance, as if the source was in the center.

The plot after interpolation and distance correction is shown in Figure 21c. Visually comparing Figures 21c and 21d reveals similar trends, with peak noise at 0° polar angle and a 12 dB decrease toward the edge of the arc. Slight differences are due to the geometric resolution available at various points on the contour, as shown in Figure 20. For the plots shown in Figures 21c and 21d, this difference was within ± 2 dB. While this method has varying degrees of interpolation error based on the deviation between ideal and measured position, it is a useful tool for visualization of acoustic trends and directivity effects. It can be used when the source is not located in the center of the measurement arc due to hardware constraints, or for cases where multiple sources are present.

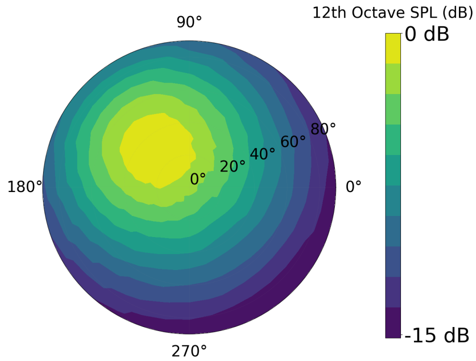

(a) Original measurement with 18-inch displacements toward 90° and 180°.

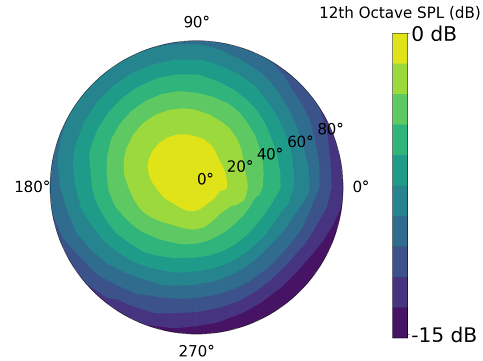

(b) After interpolation to desired Φ and θ is applied.

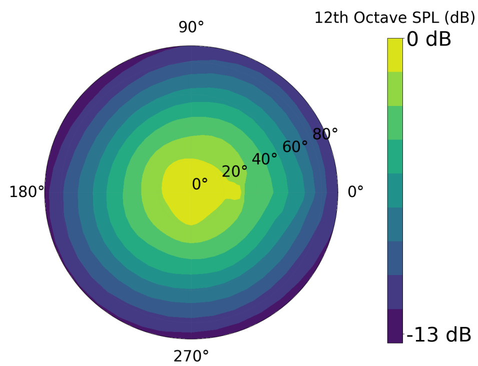

(c) After interpolation and distance correction is applied.

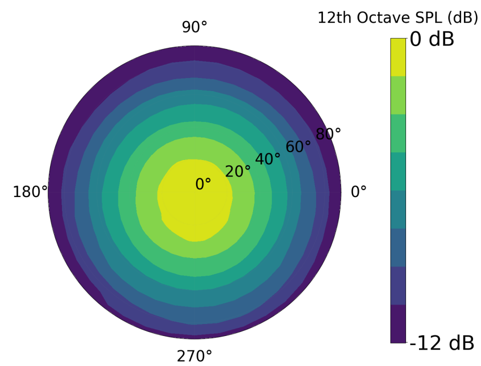

(d) Measured results for speaker located in center of array.

Figure 21. Recentering algorithm example for off-center speaker case, one-twelfth-octave band SPL centered around 4 kHz.

5 Concluding Remarks

The High Resolution Traversing Microphone Array (HiRTMA) represents a significant advancement in the ability to capture high-resolution hemispherical acoustic measurements within the anechoic chamber of the Structural Acoustics Loads and Transmission (SALT) Facility at the NASA Langley Research Center. The system provides an efficient method for acquiring directivity data, improving upon the spatial resolution limitations of traditional stationary microphones and microphone arrays. From an operational perspective, the HiRTMA significantly changes experimental capabilities of the SALT Facility. The motorized traversing system significantly reduces acquisition time when compared to manual repositioning methods, enabling full-hemisphere directivity studies in a similar timeframe of stationary studies with limited resolution.

The process of integrating the HiRTMA into experimental workflows required careful consideration of system design, control mechanisms, and measurement protocols. The initial validation tests with well-documented noise sources demonstrated that the system functions as intended, providing reliable acoustic data consistent with manufacturer specifications and existing measurement techniques. Additionally, tests with various signal processing approaches revealed further refinements that could enhance measurement accuracy and usability in future studies.

These findings establish HiRTMA's capability for improving the characterization of complex sound fields relevant to NASA's acoustics research portfolio. Additionally, the measurement capabilities now available at SALT create new opportunities for collaboration with industry partners seeking to validate computational models or evaluate noise reduction technologies under controlled laboratory conditions. As future studies incorporate the HiRTMA into a broader range of experiments, continued refinements in data acquisition and processing will further expand its applicability. The insights gained from this work establish a foundation for future research using the HiRTMA to support NASA's ongoing efforts in aircraft noise reduction and acoustic model validation.

6 Acknowledgments

This research was conducted in support of the NASA Advanced Air Transport Technology Project of the NASA Advanced Air Vehicles Program (AAVP). The authors would like to thank technicians Jaye Moen and Owen Medford for their skilled technical assistance while assembling and debugging the HiRTMA. The authors would also like to acknowledge the students of the Virginia Polytechnic Institute and State University who created the HiRTMA - Joey Eastman, Aleks Kalman, Matt Emmons, Max Koschnitzke, Matthew Lyles, and Logan Stevenson, as well as their advisor, Dr. Chris Fuller.

References

1. Daniel Sutliff. Advanced Noise Control Fan: A 20 - Year Retrospective of Contributions to Aeroacoustics Research. *NASA Special Publication*, SP-2019-643, 2019.

2. Natasha Schatzman and Douglas Boyd. A Brief History of Rotorcraft Aeroacoustics. In *6th Decennial VFS Aeromechanics Specialists' Conference*, Santa Clara, CA.

3. Brenda Henderson and Dennis L. Huff. A History of Jet Noise Research at the National Aeronautics and Space Administration. *The Journal of the Acoustical Society of America*, 150(2):1346–1369, August 2021.

4. K Joshua Bodon. *Development, Evaluation, and Validation of a High-Resolution Directivity Measurement System for Played Musical Instruments.* Thesis, Brigham Young University, 2016.

5. Samuel Bellows. *Acoustic Directivity: Advances in Acoustic Center Localization, Measurement Optimization, Directional Modeling, and Sound Power Spectral Estimation.* Dissertation, Brigham Young University, 2023.

6. Martin Pollow, Gottfried Behler, and Bruno Masiero. Measuring Directivities Of Natural Sound Sources With a Spherical Microphone Array. In *Ambisonics Symposium*, Graz, Austria, 2009.

7. Joey Eastman, Aleks Kalman, Matt Emmons, Max Koschnitzke, Matthew Lyles, and Logan Stevenson. High Resolution Traversing Microphone Array. In *NASA Acoustics Technical Working Group*, Hampton, VA, April 2022.

8. John Buck, Michael Daniel, and Andrew Singer. *Computer Explorations in Signals and Systems Using MATLAB®*. Prentice Hall, Upper Saddle River, NJ, second edition, 2002.

9. Petre Stoica and Randolph Moses. *Spectral Analysis of Signals*. Prentice Hall, Upper Saddle River, NJ, 2005.

10. Ferdinand Grosveld. Characteristics of the Structural Acoustic Loads and Transmission (SALT) facility at NASA Langley Research Center. *The Journal of the Acoustical Society of America*, 104, 1998.

11. Steve Rizzi, Randolph Cabell, and Albert Allen. Recent enhancements to the NASA Langley Structural Acoustics Loads and Transmission (SALT) facility. *International Conference on Recent Advances in Structural Dynamics*, July 2013.

12. Method for Calculation of the Absorption of Sound by the Atmosphere S1.26-1995. In *American National Standards Institute*, July 1995.

13. Clifton Horne and Nathan Burnside. Initial Calibrations and Wind Tunnel Test Results for an In-Flow Reference Array Using New In-Flow Acoustic Sources in Four Array Mount Configurations. In *AIAA AVIATION Forum*, Atlanta, GA, June 2018.

14. Bruel and Kjaer. Product Data: Reference Sound Source Type 4204. URL: https://www.bksv.com/-/media/literature/Product-Data/bp0263.ashx.

15. NTi Audio. Product Data: Dodecahedron Speaker Set. URL: https://www.nti-audio.com/Portals/0/data/en/NTi-Audio-Dodecahedron-Speaker-Set-User-Guide.pdf.